Appl Phys B (2011) 105:857–862
DOI 10.1007/s00340-011-4703-0

Applied Physics B
Lasers and Optics

Highly efficient bipolar connecting layers for tandem organic light-emitting devices

L. Niu · Y. Guan · C. Kong · Y. Cui · Y. Ren · S. Tao · J. Zhou · J. Yu

Received: 27 January 2011 / Revised version: 11 April 2011 / Published online: 8 September 2011

Abstract A highly efficient tandem organic light-emitting device (OLED) has been fabricated by using an effective bipolar connecting layer structure. The connecting layers were made up of a layer of magnesium (Mg): 2,7-dipyrenyl-9,9-diphenyl fluorene (N-DPF) and a layer of tungsten trioxide (WO_3). Such a connecting layer structure permits efficient opposite holes and electrons flowing into two adjacent emitting units. The current efficiency of the two-unit tandem device can be dramatically enhanced by more than four times compared with that of the conventional single-unit device. At 60 mA/cm^2, the current efficiency of the tandem OLED using the connecting layers of Mg: N-DPF/WO_3 was about 8.15 cd/A. The results can be marked as a breakthrough approach to improve the current efficiency and brightness of OLEDs. Furthermore, a model of the carrier tunneling into light-emitting units is proposed based on carrier balance and field-assisted tunneling. It indicates that the connecting layer structure functions as the origin of high efficiency for the tandem OLEDs.

L. Niu · S. Tao · J. Zhou · J. Yu
State Key Laboratory of Electronic Thin Films and Integrated Devices, School of Optoelectronic Information, University of Electronic Science and Technology of China, Chengdu 610054, China

L. Niu · Y. Guan · C. Kong · Y. Cui · Y. Ren
Key Laboratory of Optical Engineering, College of Physics and Electronic Engineering, Chongqing Normal University, Chongqing 400047, China

L. Niu (✉)
Department of Materials Science and Engineering, University of Tennessee, Knoxville, TN 37996, USA
e-mail: lniu2@utk.edu

L. Niu
e-mail: prof_niu@yahoo.cn

1 Introduction

Organic light-emitting devices (OLEDs) have been intensely researched due to their promising application in next-generation high-resolution, full-color, and active-matrix displays. They can emit various colors by using a wide selection of organic phosphorescent or fluorescent compounds. Various green, blue, and red OLEDs with high current efficiency, low power consumption, and long operational life have been demonstrated, and their commercialization is well underway [1]. Recently, many researchers have been devoted to the development of a tandem OLED owing to its prospect for enhancing the current efficiency, higher luminance, and conveniently tuning the emission spectra of devices through tandem units emitting different colors [2–9]. A typical tandem OLED is made up of vertically tandem multiple emissive units with connecting layers (CLs). The major challenge in tandem OLEDs is to prepare the efficient CLs between emitting units so that the current can smoothly flow through without facing substantial barriers. CLs also serve as charge-generation layers to produce electron and hole injections into suitable molecular energy levels of adjacent emission units [3]. All the reported CLs are like conventional p–n junctions, which in general consist of an electron-injecting conductive layer (n-type layer) for opposite electron injection into the lower unit and a hole-injecting conductive layer (p-type layer) for hole injection into the upper unit. For instance, a p-type layer in CLs is usually formed by metal oxides, such as indium–tin oxide (ITO) [5, 6], V_2O_5 [7], WO_3 [8], MoO_3 [9, 10], or an organic hole-transporting layer doped with a Lewis acid (e.g. $FeCl_3$: NPB) [11]; while the n-type layer is typically prepared by doping an electron-transporting layer with an active metal with low work function, such as Cs [5, 7, 12], Li [7, 10, 11], and Mg [8, 13–15]. It seems that both p- and n-type layers are

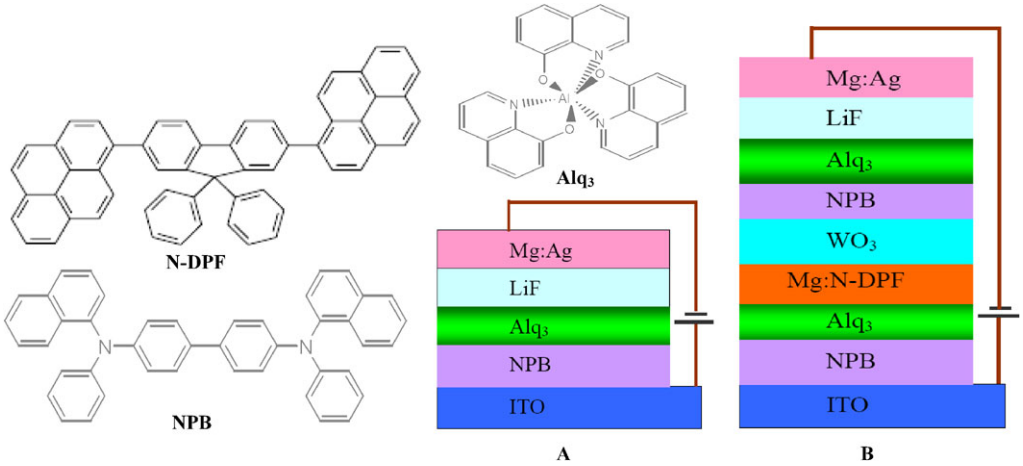

Fig. 1 Molecular chemical structures of the materials used and schematic diagrams of the device structures

necessary. Moreover, the current efficiency of a two-unit tandem device is usually twice that of the conventional single-unit device. However, few have been reported whether other types of doped layers can realize the function of CLs and obtain more than twice the efficiency of the conventional single-unit device in a two-unit tandem device.

In the present work, we fabricated a tandem OLED by using effective CLs with bipolar 2,7-dipyrenyl-9,9-diphenyl fluorene (N-DPF), which was synthesized by our team [16, 17]. The two-unit tandem device has been experimentally realized with a very high current efficiency, four times that of a single-unit OLED. A model of the carrier tunneling into light-emitting units is proposed based on carrier balance and field-assisted tunneling. It indicates that the effective bipolar CLs function as the origin of high efficiency for the tandem OLED.

In order to demonstrate the effectiveness of the bipolar CLs, we fabricated two types of devices. The configurations of the single electroluminescent (EL) unit referenced conventional device A and the tandem device B are as follows:

Device A: ITO/EL unit/LiF/Mg:Ag.
Device B: ITO/EL unit/N-DPF: Mg/WO_3/EL unit/LiF/Mg:Ag.

The tandem OLED has two standard EL units connected by a CL structure of N-DPF:Mg/WO_3. Each unit consisted of a hole-transporting layer of N,N′-bis-(1-naphthyl)-N,N′-diphenyl-1,1′-biphenyl-4,4′-diamine (NPB) and an electron-transporting green emissive layer of 8-tris-hydroxyquinoline (Alq_3). The chemical structure of the materials and schematic diagrams of the device structures are shown in Fig. 1.

2 Experimental

The substrates used in the present study were ITO-coated glass. The sheet resistance and thickness of the ITO layer were 42 Ω/□ and 110 nm, respectively. The ITO coated glass substrates were first ultrasonically cleaned in acetone, chloroform, and deionized water in this sequence. After cleaning, the substrates were dried in an oven at 125°C for 2 h. Prior to the deposition of organic compounds, the substrates were treated with oxygen plasma for 45 s. After the oxygen plasma treatment, the substrates were loaded into an OLED chamber, which is operated at a base pressure of 2×10^{-4} Pa. WO_3, N-DPF, NPB, Alq_3, LiF, and Mg:Ag (10:1 mass ratio) electrodes were thermally deposited without breaking the vacuum, respectively. The deposition rate and film thickness were monitored in situ using a quartz crystal monitor connected to a frequency meter near the ITO substrates during the deposition. The organic films, LiF, and electrode layers were deposited at rates of 0.2 nm/s, 0.01 nm/s, and 0.4 nm/s, respectively. The thicknesses of NPB, Alq_3, LiF, and Mg:Ag were 40 nm, 50 nm, 1 nm, and 200 nm, respectively. The CL thickness (Mg: N-DPF/WO_3) was 12 nm. Although these parameters might not be the best in view of achieving highest current efficiency, it was enough to demonstrate the effectiveness of the CLs. A computer-controlled KEITHLEY 2400 and a Spectra Scan PR 650 were used to measure the luminance–current–voltage (L–I–V) curves and EL spectra of the devices. All these measurements were made under ambient atmosphere at room temperature. The current–voltage characteristics were all measured in the forward bias direct current (DC) voltage mode. The operating voltage was defined as the voltage when emitted light is first detected. The standard of light first resolved is around 1 cd/m^2 in our experimental setup.

3 Results and discussion

Figure 2a exhibits the plots of the current intensities versus applied voltage for devices A and B. At 1 mA, the driving

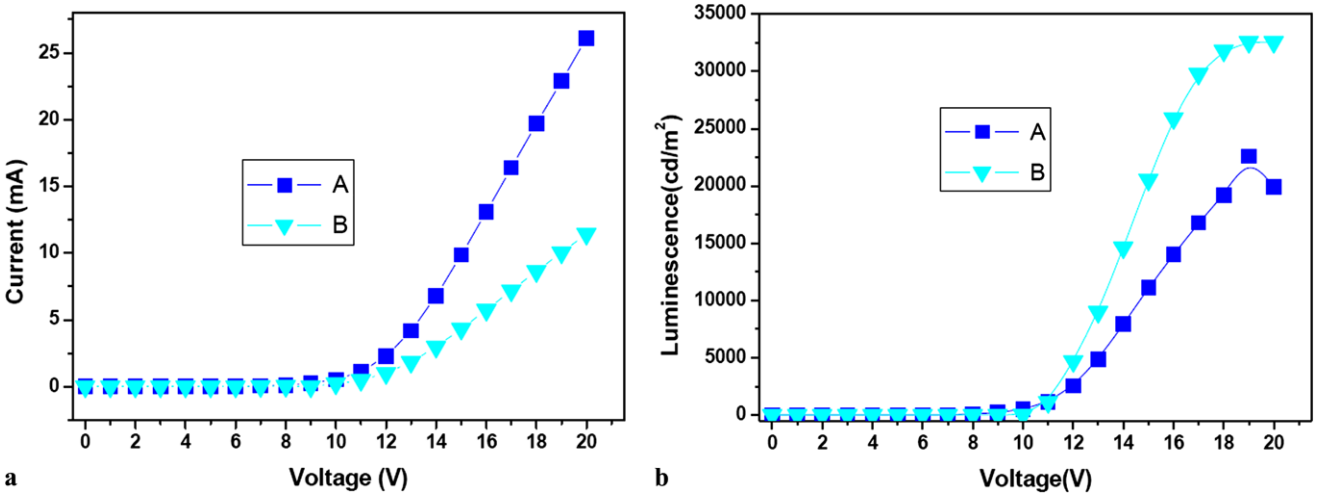

Fig. 2 (**a**) Typical current intensities versus voltage and (**b**) characteristics of luminance versus voltage of devices A and B: *rectangles*—A, *triangles*—B

voltages of devices A and B are about 8 V and 11 V, respectively. As expected, the driving voltage of device B is much higher than device A due to the large vertical tandem structure. It should be also noted, as shown in Fig. 2b, that devices A and B start to emit light at 5 V and 10 V, respectively. It is obviously shown that the operating voltage of device B is two times that of device A. The luminances from the devices A and B reach the maximum luminances of 22 600 cd/m^2 at 19 V and 32 500 cd/m^2 at 20 V, respectively.

Figure 3 shows the curves of current efficiencies versus current density of the devices. Clearly, the current efficiency is significantly improved for the tandem device B. At the injection current density of 60 mA/cm^2, the current efficiencies for devices A and B are 1.97 and 8.15 cd/A, respectively. These values clearly demonstrate that the two-EL-unit tandem architecture effectively improves the current efficiency. However, the notable weakness of the tandem device is its high driving voltage. As shown in Fig. 2b, the driving voltage of the tandem device B is higher than the conventional device A, which is attributed to the thicker organic layers and the larger series resistance of the CLs. Nevertheless, our tandem device B exhibits more than 400% improvement in current efficiency as compared to the referenced conventional device A.

Based on the above experimental results, it is evident that device B using Mg: N-DPF/WO_3 as the CLs shows the obvious enhancement of EL current efficiency. The performance of tandem device B critically depends on the effectiveness of the connecting layers. Therefore, an understanding of the underlying working mechanism of device B is essential to achieve an optimal device performance.

Emission in a conventional OLED originates from the recombination of carriers (holes and electrons) that are injected from external electrodes. In device A, holes are injected from the transparent ITO anode to a hole-transporting

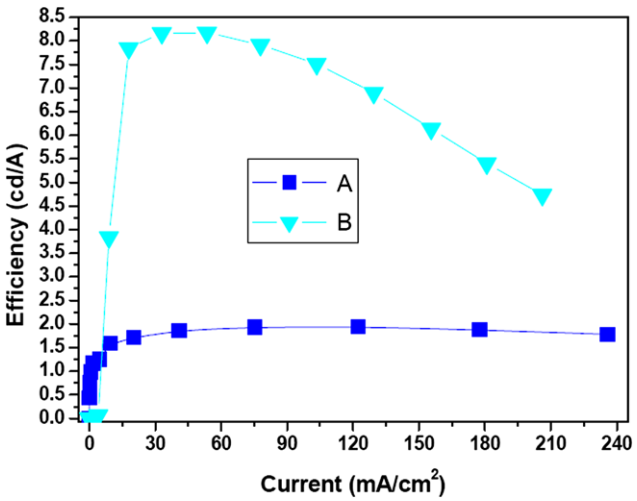

Fig. 3 Characteristics of current efficiency versus current density: *rectangles*—A, *triangles*—B

layer and holes reach an emitting zone through this hole-transporting layer. Electrons, on the other hand, are injected from the Mg:Ag cathode to an electron-transporting layer and travel to the same emissive zone. Electrons and holes recombine at the emissive zone to form singlet excited states, followed by light emission [18]. Conceptually, the configuration of the tandem OLED is like electrically connecting OLEDs in series. Therefore, the straightforward consideration of forming a connecting layer structure is to directly take the place of the ITO anode of the upper unit on top of the Mg:Ag cathode of the lower unit. But, some additional electrons and holes in tandem device B are generated within the CLs and are injected toward the adjacent electron-transporting layer and hole-transporting layer, respectively [3]. Figure 4a shows the energy-level schematic

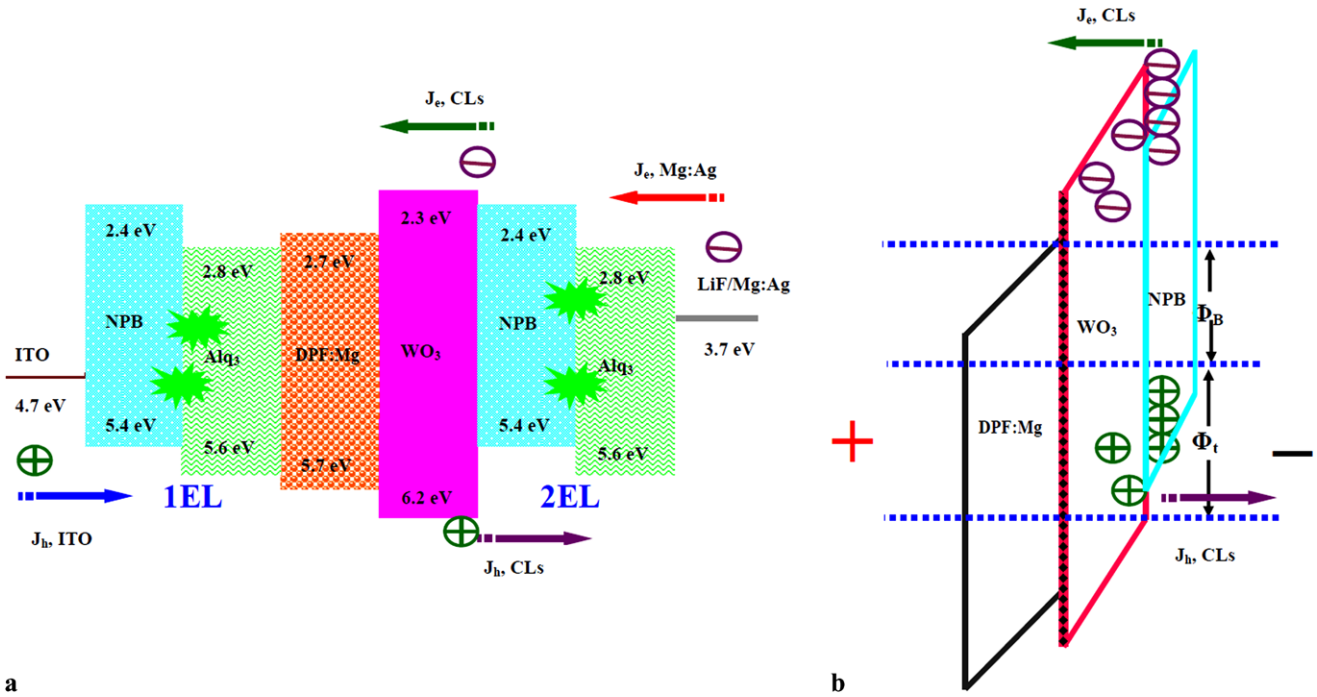

Fig. 4 (**a**) Energy-level schematic diagram of the tandem device B; (**b**) energy levels of CLs in the proposed field-assisted tunneling model

diagram of the tandem device B. The arrows point out the carrier-injection direction, with $J_{\mathrm{h,\,ITO}}$, $J_{\mathrm{e,\,Al}}$, and $J_{\mathrm{e(h),\,CLs}}$ indicating carriers (electrons or holes) injected from ITO, Al, and CLs, respectively. At the interface of NPB/WO_3, a large dipole leads to a downward shift of the vacuum level from WO_3 to the organic film, and the Fermi level is pinned close to the highest occupied molecular orbital (HOMO) level of NPB. Under the applied electric field, electrons can be effectively transferred from the HOMO level of NPB to the conduction band (CB) of WO_3. Meanwhile, the Mg: NDPF layer facilitates efficient carrier injection into the appropriate carrier-transporting layers of the adjacent emission units. Kröger et al. [19] also demonstrated that the mechanism of doped organic/organic CLs heterostructures can be explained by a field-induced tunneling process from the HOMO state of a p-doped layer to the lowest unoccupied molecular orbital (LUMO) state of an n-doped layer. Electron injection occurs via excited electrons into traps located at energy, Φ_t, above the valence-band maximum (VBM) of WO_3, as shown in Fig. 4b. This is followed by field-assisted tunneling through the thin depletion region of the adjacent doped organic layer.

The external EL quantum current efficiency of an OLED is given as a product of several factors [20], as shown in (1).

$$\eta_{\mathrm{EL}} = \eta_{\mathrm{PL}}\eta_{\mathrm{S}}\gamma\eta_{\mathrm{out}} \tag{1}$$

where η_{PL} is the photoluminescence quantum efficiency, η_{S} is the efficiency for the yield of singlet excitons, γ is the carrier balance factor, and η_{out} is the extraction efficiency. The definition of the carrier balance factor is shown as (2).

$$\Gamma = j_{\mathrm{r}}/j. \tag{2}$$

In the first EL unit 1_{EL}, the carrier balance factor is

$$\gamma_1 = j_{\mathrm{r1}}/j_1.$$

The recombination current density and the total current density in the external circuit are shown as (3) and (4).

$$j_{\mathrm{r1}} = j_{\mathrm{h}} + j_{\mathrm{h,CLs}} - j'_{\mathrm{h1}} = j_{\mathrm{e,CLs}} - j'_{\mathrm{e1}}, \tag{3}$$

$$j_1 = j_{\mathrm{h}} + j_{\mathrm{h,CLs}} + j'_{\mathrm{e1'}} = j_{\mathrm{e,CLs}} + j'_{\mathrm{h1}}. \tag{4}$$

In the second EL unit 2_{EL}, the carrier balance factor is

$$\gamma_2 = j_{\mathrm{r2}}/j_2.$$

And, the recombination current density in EL unit 2_{EL} and the total current density in the external circuit are shown as (5) and (6).

$$j_{\mathrm{r2}} = j_{\mathrm{h}} + j_{\mathrm{h,CLs}} - j'_{\mathrm{h2}} = j_{\mathrm{e,CLs}} - j'_{\mathrm{e2}}, \tag{5}$$

$$j_2 = j_{\mathrm{h}} + j_{\mathrm{h,CLs}} + j'_{\mathrm{e2'}} = j_{\mathrm{e,CLs}} + j'_{\mathrm{h2}}, \tag{6}$$

where j_{e}, and j_{h} are the injected electron and hole current densities from external electrodes, respectively. The primed quantities denote the respective fractions reaching the counter electrode without recombining. $j_{\mathrm{e(h),CLs}}$ are

electron and hole current densities from CLs; $j'_{h,e}$ is the hole and electron leakage current density. Electrons are minority carriers and holes are majority carriers in the first EL unit 1_{EL}. However, electrons are majority carriers and holes are minority carriers in the second EL unit 2_{EL}. Because bipolar N-DPF has good transporting properties for both electrons and holes in the tandem device B, excess holes from EL unit 1_{EL} and redundant electrons from EL unit 2_{EL} are easy to flow into the next needed EL zone to be best utilized. Moreover, the barrier height between the LUMO of N-DPF and the CB of WO_3 is 0.4 eV and between the HOMO of N-DPF and the VBM of WO_3 is 0.5 eV. These low barriers are easy for electrons and holes to tunnel through. As a result, the carrier balance factor γ is close to unity. According to (1), (2), (3), (4), (5), and (6), this is achieved if both j'_h and j'_e vanish. Therefore, a fourfold enhancement for the current efficiency in the tandem device B is mainly due to the bipolar charge transporting properties of N-DPF. Chang et al. [21] and Cho et al. [22] also achieved more than four times enhancement for current efficiency with clever ways in their published papers. On the other hand, at an applied voltage V, the electron ($j_{e,CLs}$) and hole ($j_{h,CLs}$) current densities in the CLs are as follows:

$$j_{e,CLs} = j_{h,CLs} = q v_e N_t f P(V), \tag{7}$$

where $f = 1/\{1+\exp[q\Phi_t/kT]\}$ is the Fermi–Dirac function, q is the elementary charge, T is the absolute temperature, k is Boltzmann's constant, Φ_t is the trap level above the VBM of WO_3, v_e is the electron thermal velocity [23, 24], N_t is the concentration of traps, and $P(V)$ is the tunneling probability over an interface barrier of height Φ_B [25]. Now we can get $P(V)$ as (8).

$$P(V) = \exp\left[\frac{-4\Phi_B^{\frac{3}{2}}\sqrt{2qm_s}}{3\hbar E(V)}\right]. \tag{8}$$

Here, $E(V)$ is the electric field at voltage V, m_s is the electron effective mass in the organic compounds, and $\hbar$ is Planck's constant divided by 2π.

The electron ($j_{e,CLs}$) and hole ($j_{h,CLs}$) current densities depend on the electric field $E(V)$ but not on the type of excitation. According to (7) and (8), $j_{e,CLs}$ and $j_{h,CLs}$ will be increased with increasing $E(V)$. So, the current efficiency increased with increasing applied voltage from 1 mA/cm^2 to 60 mA/cm^2 in Fig. 3. However, the current efficiency decreased beyond 65 mA/cm^2. At that time, the applied voltage is very high; it was suggested that the dominating factor might be the shift of the carrier recombination zone close to the electrode contact, where serious luminescence quenching could happen.

The normalized EL spectra of devices A and B at the maximum current efficiency are shown in Fig. 5. Commission Internationale de L' Eclairage chromaticity coordinates are ($x = 0.31$, $y = 0.54$) for device A and ($x = 0.30$, $y = 0.56$) for device B. The peaks of emitting light originating from the Alq_3 fluorescent emitter in conventional and tandem devices are 516 nm and 524 nm, respectively. But, the full width at half-maxima of devices A and B are 104 nm and 106 nm, respectively. The EL emission peak of the tandem device B is slightly shifted toward the long-wavelength range compared with the conventional device A. This indicates that the microcavity effect still exists in the tandem device B [26].

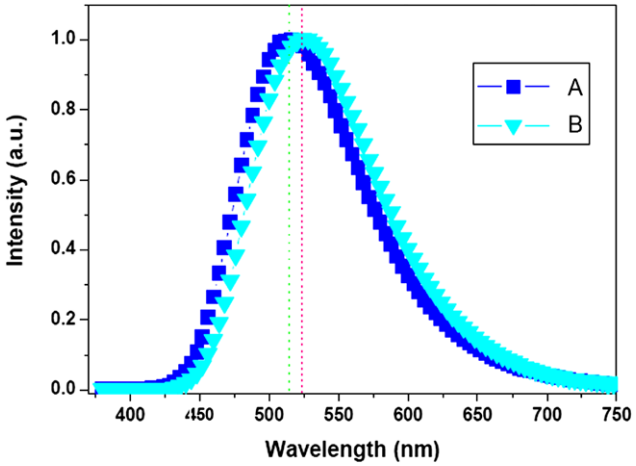

Fig. 5 Normalized EL spectra of devices A and B: *rectangles*—A, *triangles*—B

4 Conclusion

In conclusion, it has been demonstrated that the device consisting of two EL units connected electrically in series using Mg: N-PDF/WO_3 as the effective bipolar CLs is useful in producing high-efficiency and high-brightness tandem OLEDs. Such a CL structure, which can be easily fabricated by sequential thermal evaporation, permits efficient opposite holes and electrons flowing into two adjacent emitting units and gives superior electrical and optical performances in tandem devices. It is anticipated to provide a new approach to the design and fabrication of highly efficient tandem OLEDs for future applications, such as in televisions and illumination devices.

Acknowledgements This work was supported by the National Natural Science Foundation of China (Grant No. 60806047), the China Postdoctoral Science Foundation (Grant Nos. 20100481376 and 20100471667), the Natural Science Foundation Project of CQ CSTC (Grant Nos. 2009BB2237 and cstc2011jjA1086), the Research Programs for Science and Technology of Chongqing Municipal Education Commission (Grant Nos. KJ100613 and KJ080816), the Foundation for the Creative Research Groups of Higher Education of Chongqing (Grant No. 201013), and the Natural Science Foundation of Chongqing Normal University (Grant Nos. 07XLB015 and 08XLS12).

References

1. C. Jenny, L. Guglielmo, Nat. Photonics **4**, 438 (2010)
2. R. Madhava, T. Huang, Y. Su, Y. Huang, Devices J. Electrochem. Soc. **157**, H69 (2010)
3. Q. Bao, J. Yang, Y. Li, J. Tang, Appl. Phys. Lett. **97**, 063303 (2010)
4. L. Niu, Y. Guan, Y. Ren, C. Kong, Y. Ma, Y. Liang, Sci. China Ser. E – Tech. Sci. **52**, 95 (2009)
5. J. Sun, X. Zhu, H. Peng, M. Wong, H. Kwok, Appl. Phys. Lett. **87**, 093504 (2005)
6. P. Burrows, S. Forrest, S. Sibley, M. Thompson, Appl. Phys. Lett. **69**, 2959 (1996)
7. F. Guo, D. Ma, Appl. Phys. Lett. **87**, 173510 (2005)
8. C. Chang, J. Chen, S. Hwang, C. Chen, Appl. Phys. Lett. **87**, 253501 (2005)
9. C. Chen, Y. Lu, C. Wu, E. Wu, C. Chu, Y. Yang, Appl. Phys. Lett. **87**, 241121 (2005)
10. H. Kanno, R. Holmes, Y. Sun, S. Cohen, S. Forrest, Adv. Mater. **18**, 339 (2006)
11. L. Liao, K. Klubek, C. Tang, Appl. Phys. Lett. **84**, 167 (2004)
12. T. Cho, C. Lin, C. Wu, Appl. Phys. Lett. **88**, 111106 (2006)
13. T. Tsutsui, M. Terai, Appl. Phys. Lett. **84**, 440 (2004)
14. C. Law, K. Lau, M. Fung, M. Chan, F. Wong, C. Lee, S. Lee, Appl. Phys. Lett. **89**, 133511 (2006)
15. M. Chan, S. Lai, K. Lau, M. Fung, C. Lee, S. Lee, Adv. Funct. Mater. **17**, 2509 (2007)
16. S. Tao, C. Lee, S. Lee, Appl. Phys. Lett. **91**, 013507 (2007)
17. S. Tao, L. Niu, J. Yu, Y. Jiang, X. Zhang, J. Lumin. **130**, 70 (2010)
18. T. Tsutsui, S. Lee, K. Fujita, Appl. Phys. Lett. **85**, 852382 (2004)
19. M. Kröger, S. Hamwi, J. Meyer, T. Dobbertin, T. Riedl, W. Kowalsky, H.-H. Johannes, Phys. Rev. B **75**, 235321 (2007)
20. W. Brütting, S. Berleb, A. Mück, Org. Electron. **2**, 1 (2001)
21. C. Chang, S. Wen, C. Chen, J. Fang, Jpn. J. Appl. Phys. **43**, 6418 (2004)
22. T. Cho, C. Lin, C. Wu, Appl. Phys. Lett. **88**, 111106 (2006)
23. S. Fleischer, P. Lai, J. Appl. Phys. **72**, 5711 (1992)
24. X. Qi, N. Li, R. Stephen, J. Appl. Phys. **107**, 014514 (2010)
25. D. Sathaiya, S. Karmalkar, J. Appl. Phys. **99**, 093701 (2006)
26. A. Rajagopal, A. Kahn, J. Appl. Phys. **84**, 355 (1998)